

Optimal Control Measures Based on the Reconstruction of the COVID-19 Interlocality Transmission Network in Lebanon

Sara Najem^{1,2}, Stefano Monni^{1,3}, Rola Hatoum¹, Hawraa Sweidan⁴, Ghaleb Faour⁵,
Nada Ghosn⁴, Hamad Hassan⁶, and Jihad Touma^{1,2}

¹Center for Advanced Mathematical Sciences, American University of Beirut,
Beirut, Lebanon

²Department of Physics, American University of Beirut, Beirut, Lebanon

³Department of Mathematics, American University of Beirut, Beirut, Lebanon

⁴Epidemiological Surveillance Program, Ministry of Public Health, Beirut, Lebanon

⁵National Center for Remote Sensing, National Council for Scientific Research
(CNRS), Riad al Soloh, Beirut, Lebanon

⁶Faculty of Public Health, Lebanese University, Lebanon

*corresponding authors: Sara Najem (sn62@aub.edu.lb), Jihad Touma
(jt00@aub.edu.lb)

April 26, 2022

Abstract

In this paper, we study the evolution of COVID-19 in Lebanon using the data collected by the Epidemiological Surveillance Program of Lebanon's Ministry of Public Health. We develop an autoregressive model that allows us to decompose the mean number of infections into three components that describe: intra-locality infections, inter-locality infections, and infections from other sources such as travelers arriving from abroad. We observe that the inter-locality term, which we identify as a time-evolving network, drives the dynamics of the disease. Tools from network analysis are then employed to get insight into its topology. Building on this, and particularly on the centrality of the nodes of the identified network, a strategy for intervention and disease control is devised.

1 Introduction

Many studies have appeared in the literature to address a wealth of questions about the COVID-19 pandemic, covering a range of disciplines from medicine, genetics, pharmacology to social and economic sciences [1, 2]. Some of these studies have a regional focus, investigating the disease in countries, or regions of a country, while others have considered the pandemic in larger geographical contexts [3, 4, 5].

Modeling the evolution of the disease has been one of the main quantitative approaches used, especially with the goal of forecasting numbers of affected cases. It has also been at the heart of

subsequent investigations on practical aspects: from management of resources (assessment of the preparedness for disease containment and readiness of the healthcare system) to possible intervention measures (vaccination and testing strategies [6], government control measures) and their consequences [7]. The different modeling frameworks that have been applied to investigate the dynamics of COVID-19 infections, have a long history in epidemic modeling. Compartmental models (*e.g.*, SIR, SIER) are a well known class of models. They study the interplay between susceptible, infected and recovered individuals within communities, with different degrees of spatial refinement. For instance, in the so called networked compartmental models, interactions between communities are encoded in a network [8], often to identify the spatial and temporal origin of the disease [9]. In statistics, spatial/and/or temporal point processes are often employed to study the dynamics of the disease. Some models allow for the number of infections to be triggered by those at previous times, others can incorporate, as covariates, additional available information such as demographics, human mobility, and policy decisions. Some recent work on COVID-19 adopted this framework [10, 11, 12]. Epidemic models can also be recast in a standard regression framework, where the time series of infection counts are fitted by specifying a distribution for the counts and the associated conditional mean function [13, 14]. In most of these studies, of the goal is to predict and capture the spatio-temporal patterns of disease spread. Recently, this approach was implemented on COVID-19 data [3, 4, 5].

In this paper, we follow the standard regression framework as the starting point of our analysis of the COVID-19 pandemic in Lebanon. Information on the counts in the country’s different localities and on their spatial proximity are used to model the evolution of the mean function of infection counts, which we assumed to have a negative binomial distribution. Our analysis provides evidence that the inter-locality infection drives the overall transmission of the disease [15]. Then, for this reason we shift our focus to the network that governs the interaction between localities and observe that it is not purely a static spatially-dependent network but rather dynamic and time-evolving: in fact the product of time-dependent coefficients with the spatial proximity matrix. Consequently, instead of using the model for counts prediction, as commonly done, we use it for weighted network reconstruction [16]. The advantage of our method in network recovery is that it does not require any smoothness condition on the temporal data [17], nor necessitates near steady-state dynamics for the perturbation/response approaches to be applicable [18, 19, 20]. It is similar to the reconstruction framework in [21], and differs from procedures that rely on the deterministic evolution of the disease [22, 23]. We then follow the changes in the topology of the underlying recovered network resorting to tools from network dynamics. Based on these findings we recommend control measures that depend on the betweenness centrality of the nodes. This novel approach leverages the adopted stochastic modeling framework to unexplored applications in optimal disease control.

2 Model Definition

COVID-19 disease is a mandatory notifiable disease in Lebanon. On daily basis, the laboratories from the public and private sectors report the confirmed cases to the Epidemiological Surveillance Program of Lebanon’s Ministry of Public Health (ESUMOH). Later, the cases are investigated in order to get additional demographic information and health condition. The data are then archived in a national platform. Specifically, the data we have considered consist of counts of COVID-19 recorded daily in each of the 1544 localities of Lebanon from February 21, 2020 to January 20, 2022. Such localities correspond to Lebanon’s smallest statistical units called “circonscriptions foncières” or cadastral villages following the Central Administration for Statistics (CAS) nomenclature [24].

Our starting point of the analysis is a statistical model that captures the spatio-temporal dynamics of the infections, under the statistical framework discussed in [13]. Namely, we consider the number Y_{it} of infections recorded in a given locality i in a given day t , as independent, conditionally on the counts at previous times, random variables distributed according to a negative binomial distribution having a mean function decomposed into three terms as follows:

$$E(Y_{i,t}|Y_{j,t-1}, e_i) = \mu_{it} = \lambda_{it}Y_{i,t-1} + \phi_{it} \sum_{j \neq i} \omega_{ij}Y_{j,t-1} + \nu_{it}e_i. \quad (1)$$

The first two terms constitute the auto-regressive part of the model: one being the contribution to the mean infection μ_{it} in locality i at time t , due to the infections within i at the previous day, the other being the contribution to μ_{it} due to positive cases from other localities j also at the previous day. The final term accounts for all other contributions not captured by the first two, such as infected people who entered the country through the airport. For simplicity we will refer to the last term $\nu_{it}e_i$ as the component due to travel and assume that it is proportional to the size of the population e_i . The log-transforms of non-negative coefficients λ_{it} and ϕ_{it} , which quantify the contribution of the past observations to future counts, and the log-transform of the parameter ν_{it} are each modeled as a linear function of time, with a locality-specific slope to allow more flexibility across localities. Intercepts and slopes are estimated from the data. Finally, we model ω_{ji} as a power function of the geographical distance d_{ij} of the localities: $\omega_{ji} \propto d_{ij}^{-f}$. This is assumed because previous studies have shown that mobility flows are governed by power-law functions of inter-localities distances [15, 25, 26, 27]. Recommendations on possible interventions and updates on the disease evolution were sought for by the Ministry of Public Health at 20 days intervals, therefore the model of 1 that we have specified was fitted using the R package `surveillance` [14] over the intervals $[0, t]$, $t = 20 \cdot n$ for $n = 1, \dots, 35$. This allows us to follow the evolution in time of the model parameters until day 700, the last observation point.

Figure 1 displays the aggregated counts over all localities, $\sum_i Y_{i,t}$, and the fitted values over the complete time period of our study broken down into the three components of the mean function. The fit appears quite adequate. It is in fact a better fit to the data than the model with counts assumed to be Poisson-distributed, which is an indication of overdispersion in the data. A further comparison of these two models in terms of AIC value and prediction errors is provided in Table 1.

	ses	AIC
Negative Binomial	2.88	1164119
Poisson	3.65	1333453

Table 1: Comparison of the two models with the same mean function given in Equation (1) with distribution of the counts being negative binomial and Poisson. AIC is Akaike’s Information criterion. SES is the mean squared error: the mean squared difference over the localities of the observed and predicted counts at the final time point of the study

We further notice that the model of Equation (1) considers a time-lag of one day; that is, the future counts depend on the counts recorded on the previous day. Changes in the time-lag from one to a few days did not result in any noticeable difference. Figure 1 indicates that the inter-locality term has the most important contribution to the increase in the mean number of infections compared to the intra-locality and travel terms. This suggests that the inter-locality transmissions should be the main focus of analysis, and what one learns from their study would be useful for disease control.

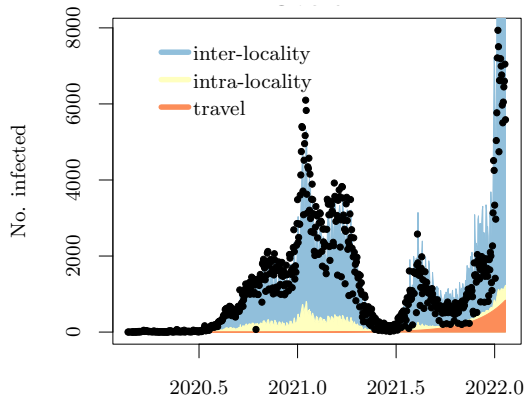


Figure 1: Data and fit under the model of Equation (1) with negative binomial distributed counts. The three colors show the decomposition of the fitted aggregate counts into travel, intra-locality, and inter-locality contributions to infections amounting to 3%, 10%, and 87% respectively.

The parameter estimates of model of Equation (1) for all 1554 localities and their errors can not be displayed in an uncluttered fashion but are available from the corresponding authors. A sample of the evolution of the inter-locality term ϕ_{it} is shown in Figure 2.

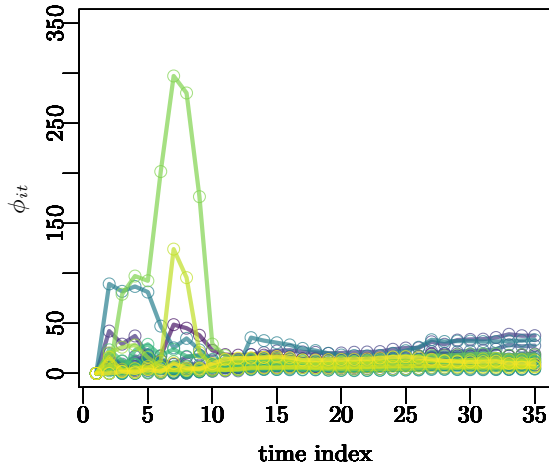


Figure 2: Time evolution of the inter-locality parameter ϕ_{it} is shown for the regions with the highest centrality (see section 3).

3 Network Characterization

As has emerged from the statistical model, the inter-locality dynamics plays the major role in determining the infection numbers. While this may seem to contradict previous studies, for example [28], on the secondary attack rate being mostly driven by household interactions, it is worth noting that infections outside households are hard to pin down, and thus this may be a limitation in such studies. We wish to focus now on the inter-locality term and study it from a different perspective. To do so, observe that the second term of mean equation (1) can be re-written as follows: $\sum_{j \neq i} A_{ij}(t) Y_{j,t-1}$, where $A_{ij}(t) = \phi_{it} \cdot \omega_{ij}$. It can be interpreted as the contribution to the cases at time t in locality i from cases from locality j at the previous day. We can suggestively think of $A = (A_{ij})$ as defining the weights of a network between localities: the transport network ω describes the traffic flow between localities, and thus predates the disease, while ϕ_{it} is the number of transported cases from i into neighboring localities. $A(t)$ explicitly depends on t since the coefficients of $\log \phi_{it}$, which are linear functions of t , and the power f in the definition of ω are estimated over each interval $[0, t]$. An example is provided in Figure 3 which is a graphical representation of $A^{(15)}(t = 300)$. The superscript 15 in the notation of A indicates that the latter was estimated on the counts data of 15 contiguous 20-day time intervals, that is the 300-day time span $[0, 20 \cdot 15]$ from February 21, 2020 to December 16th, 2020. This complex network A drives the cross-localities dynamics. We will now suggest employing some useful summary metrics for $A(t)$ and its time evolution in order to understand its properties, and accordingly prescribe adequate control measures.

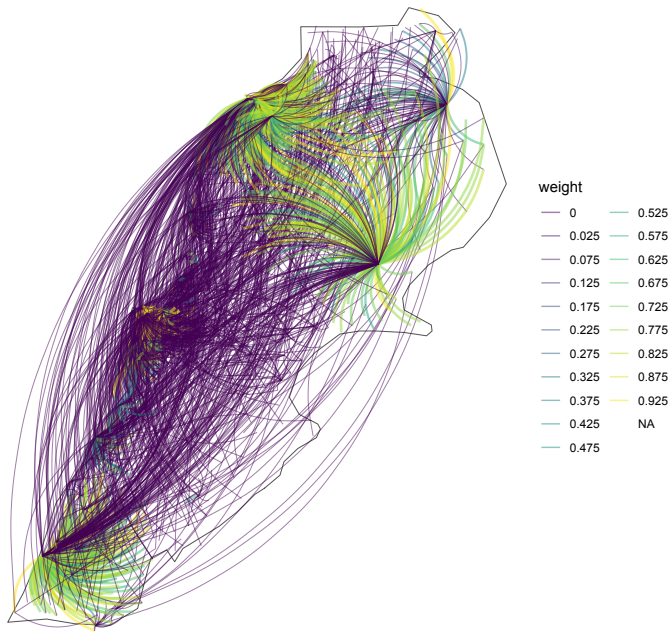


Figure 3: The network $A^{(15)}(t = 300)$ is overlaid on the map of Lebanon to illustrate its complexity. It is evaluated at the 300-th day of the pandemic using all 15 time interval of our collected data, that is the time span $[0, 20 \cdot 15]$.

One useful summary metric is the modularity, which is a measure of cluster formation in a network. More specifically, the modularity Q of a given network A is defined with respect to a given grouping of its nodes. We follow [29] where the grouping of the nodes is determined by a stochastic procedure that reveals densely connected subgraphs. An illustration of a grouping is given in Figure 4.

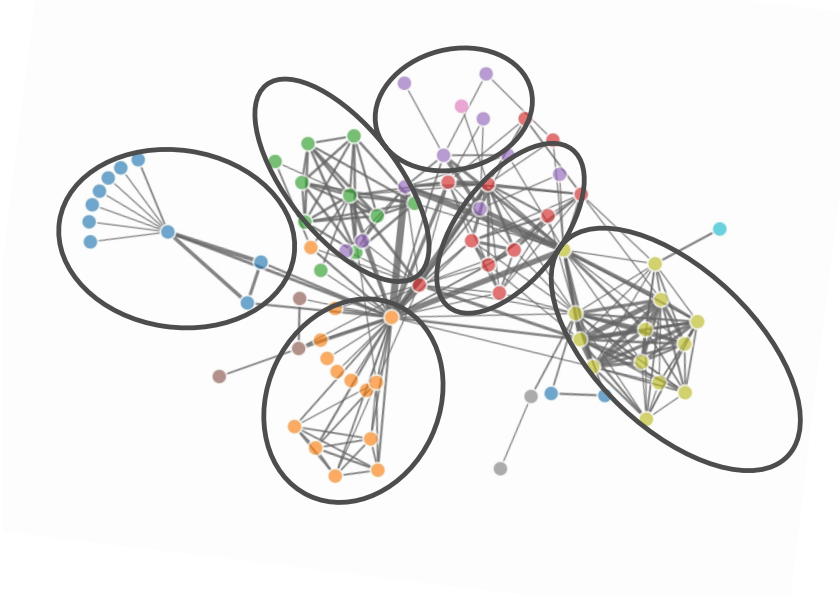


Figure 4: An example of modular network along with its detected communities (encircled) is shown. The nodes are color-coded based on their memberships to these communities.

Given this group membership, the modularity of A is then computed according to the formula:

$$Q(A) = \frac{1}{2h} \sum_{i,j} \delta(c_i, c_j) (A_{ij} - k_i k_j / (2h)),$$

where h denotes the total number of edges, k_i and k_j are the degree of nodes i and j respectively, c_i labels the group to which i belongs, and δ is the Kronecker delta. Figure 5 shows the modularities of the 35 matrices $A^{(35)}(t)$ at days $t = 20 \cdot n$ for $n = 1, \dots, 35$. The superscript n in the notation $A^{(n)}(t)$, as mentioned above, indicates that A is estimated using the counts of the $20 \cdot n$ days of the study. One can see a jump in modularity on the tenth 20-day time interval, which we will denote by I_c . This behavior may signal the onset of an emerging power-law [30]. We investigate if this is the case by analyzing two additional topological measures for the networks: mainly, the clustering coefficient and the average path length [31, 32]. These are generally used to classify networks into random, scale-free, or regular. The clustering coefficient C of a network is a measure of transitivity that counts the ratio of the number closed triplets to the number of all (closed and open) triplets. A triplet is closed if all the three connections between the three nodes exist and is open if one of the links is missing. The average path length l of a network is given by the mean distance over all pairs of vertices, where distance is the number of edges in the shortest path joining them. An illustration is shown in Figure 6. Small-world or scale-free networks (that is, networks with node degrees and

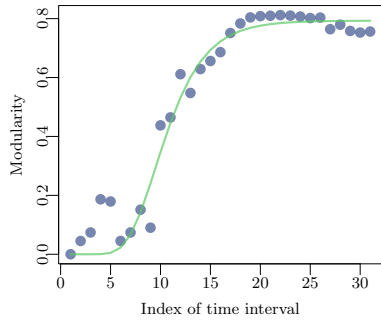


Figure 5: The modularity of the network $A^{(n)}(t)$ is shown as a function of time $t = 20 \cdot n$, with $n = 1 \dots 35$. It is measure of the quality of the division of a graph into subgraphs.

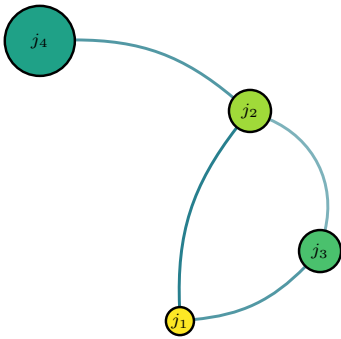


Figure 6: Example of a network with $C = 1/3$ and $l = 8/6$ is shown. It has three triplets, one of which is closed (triangle). The lengths of the paths from j_2 to all others is 1, while that from j_1 to j_4 is 2.

strengths distributed according to a power-law) are characterized by high clustering coefficients and low average path lengths compared with those of regular/ordered graphs [32, 31]. Random graphs are, on the other hand, characterized by low average path lengths and low clustering coefficients compared to regular graphs. An illustration of the three different network types is shown in Figure 7.

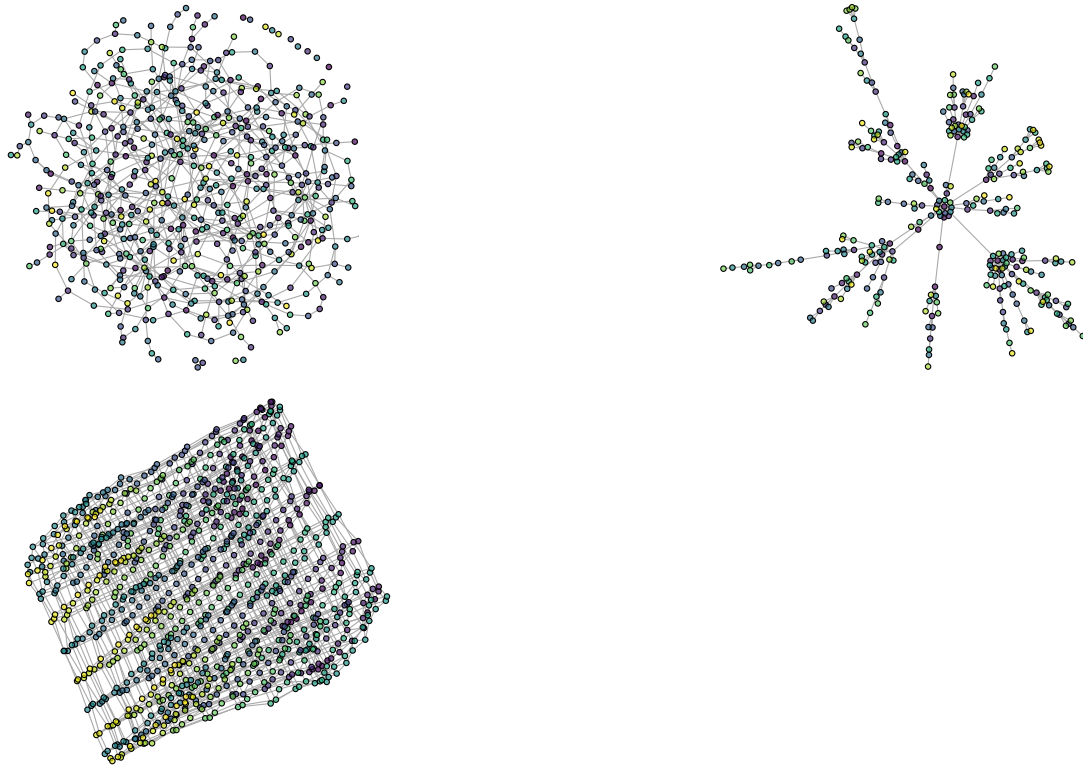


Figure 7: Examples of random, scale-free, and ordered (lattice-like) networks are shown respectively.

Figure 8 shows the clustering coefficients and the average paths lengths for the matrices $A^{(35)}(t)$. Similar behavior of both C and l was observed for all $A^{(n)}$, with $n \geq 10$. The evolution of both

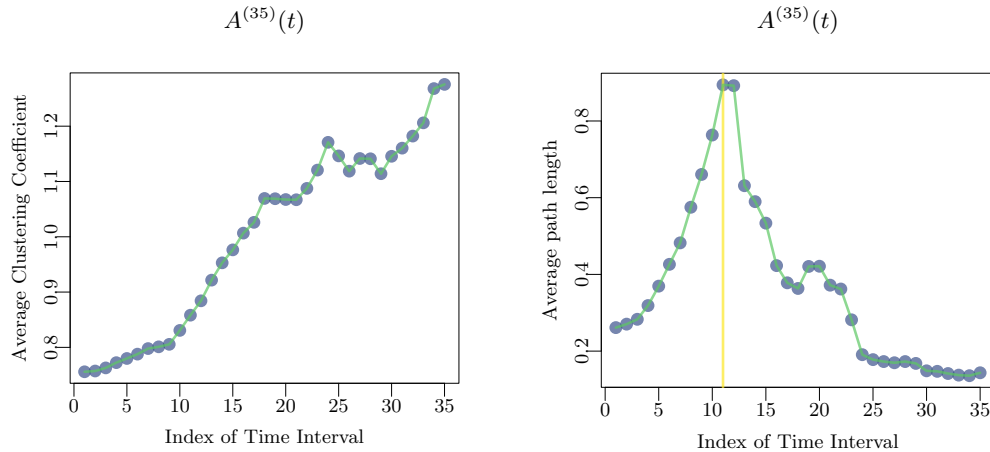


Figure 8: The figure shows the clustering coefficient and average path length for $A^{(35)}(t)$, which are the matrices estimated using the data from the start of the pandemic to the 700-th day ($35 \cdot 20$) evaluated at $t = 20 \cdot n$, where n is the index of the time intervals.

C and l gives additional evidence for a transition at a point I_c . The clustering coefficient starts suddenly to increase. At the 10-th interval there is an abrupt jump in the average path length as well at I_c (Figure 8). This is an indication of scale-freeness of the network. This property expedites the spread of epidemics unlike what would occur in ordered networks, which are characterized by a slower spread because they possess a high C and an l that scales with system size [33, 34].

To characterize the transition to scale-freeness, we now analyse the distribution of the strengths of the nodes, as additional evidence for change in the network topology at the 10-th interval I_c . A node's strength is the sum of the weights of its edges. Namely, for the i -th node:

$$s_i = \sum_j A_{ij}$$

Figures 9 and 10 show the empirical and estimated distributions of the strengths (in fact, the survival function $P(S > s)$) of $A^{(n)}(t = 20 \cdot n)$, at the time intervals $n = 1, \dots, 35$ on a log-log scale. We note that a transition occurs at $t = 20 \cdot 10$, where the distribution becomes linear, which is indicative of a power-law (Pareto distribution): $P(X \leq x) = 1 - (\beta/x)^{\alpha-1}$, for $x \geq \beta$. The exponent α and the boundary value (scale) β are estimated by maximum likelihood following [35].

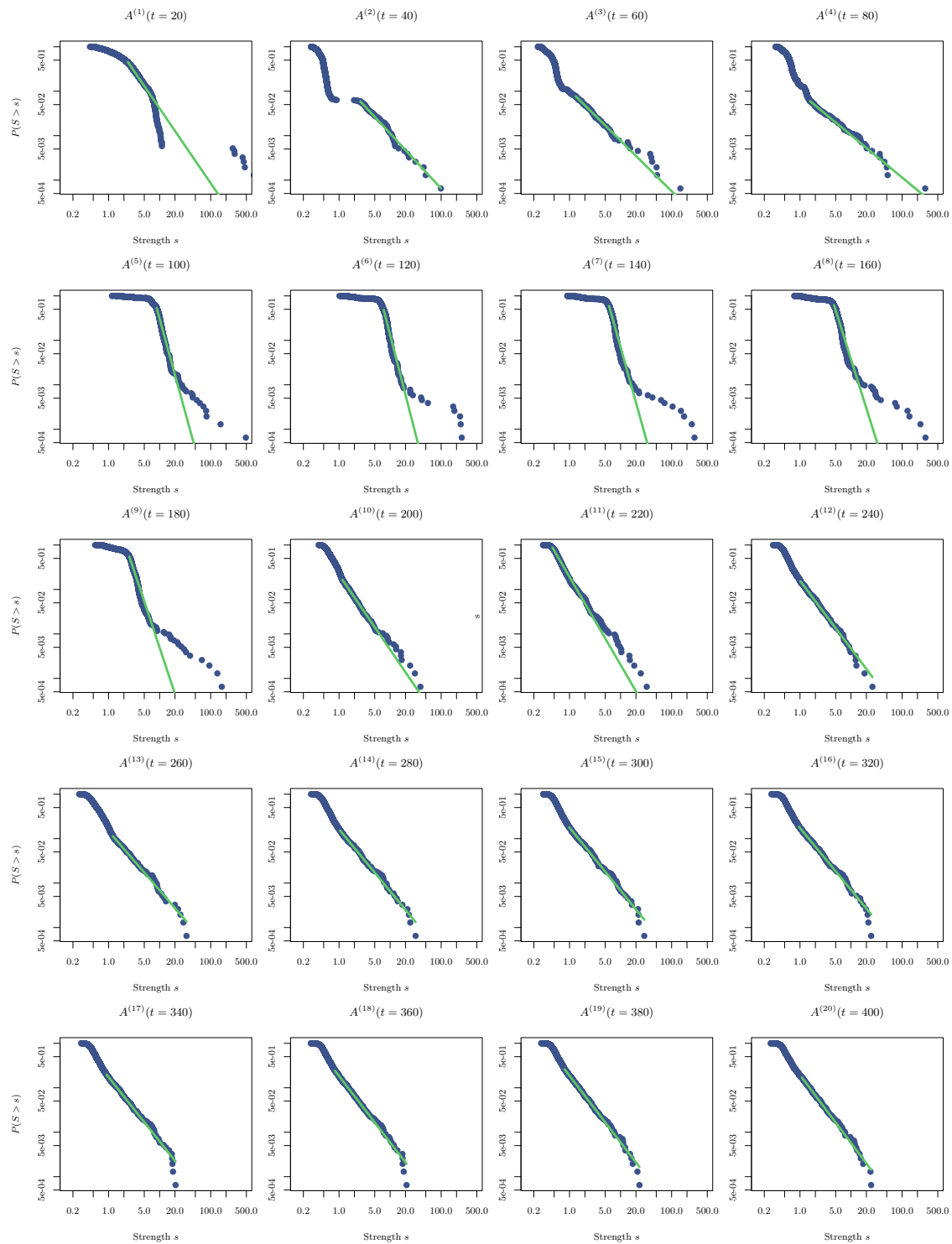


Figure 9: Empirical and estimated distributions of the strength for the matrices $A^{(n)}(t = 20 \cdot n)$ with $n = 1, \dots, 20$ are shown.

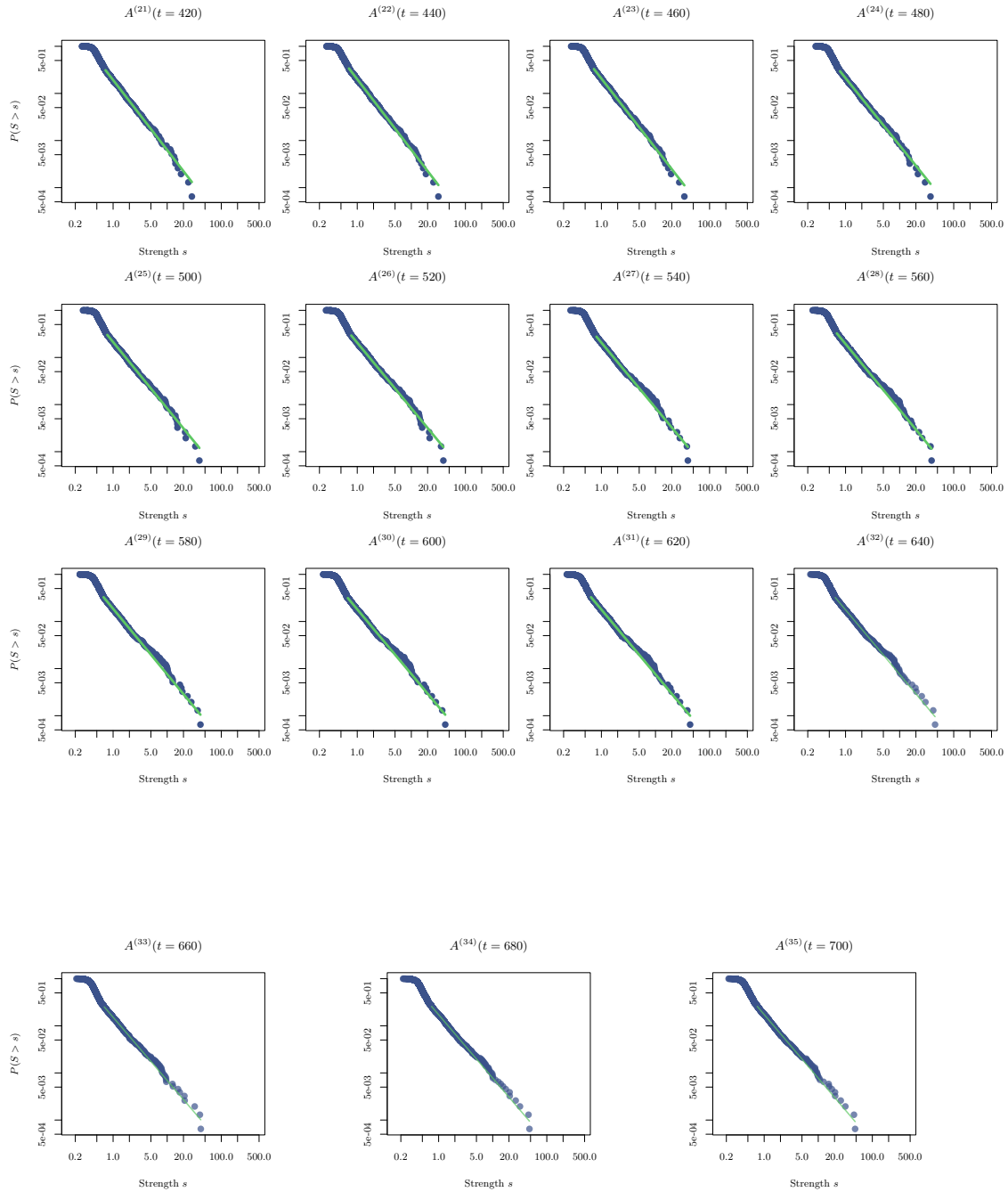


Figure 10: Empirical and estimated distributions of the strength for the matrices $A^{(n)}(t = 20 \cdot n)$ with $n = 21, \dots, 35$ are shown.

Figure 11 summarizes the estimates of the exponents for these networks and their standard errors (obtained by non-parametric bootstrap).

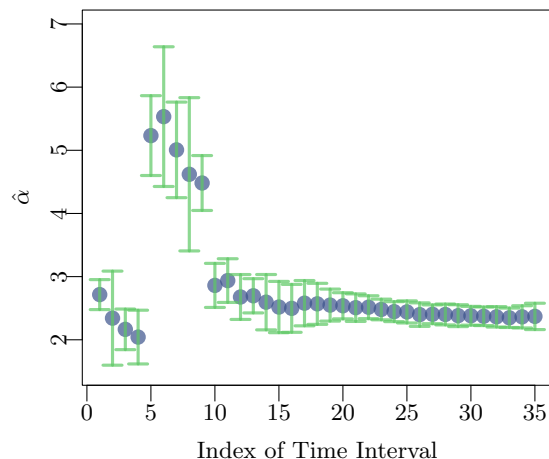


Figure 11: Estimated values $\hat{\alpha}$ of the exponent of the power-law distributions of the strengths of the nodes of the 35 matrices $A^{(n)}(t = 20 \cdot n)$, $n = 1, \dots, 35$, which are represented in Figure 9. Vertical bars indicate $\pm 2\hat{\sigma}_{\hat{\alpha}}$.

After the 180th day, that is for time intervals labeled by the index $n \geq 10$, most power-laws have very close exponents of about 2.5. This signals the stabilization of the network topology. Thus, I_C marks the onset of the emergence of the steady state network. We think that only above this point any prescription of control measures is likely to be efficient as the revealed network topology, relying on the daily counts, has stabilized. One can wonder if there is any explanation on why the stable phase has set in during this interval I_C , and not before or after it. I_C chronologically coincides with the period between August, 19, 2020, and September 7, 2020. Perhaps, the blast in Beirut which occurred on August 4th and in the following weeks of social protests, personal precaution measures (such as social distancing and wearing of masks) were compromised. Either of these occurrences may have contributed to the detected change in the network type. See the Appendix for the chronology.

4 Putting the analysis into action: Control measures

Having fully characterized the network and identified the steady-state, we now turn to a possible use of this analysis to guide an optimal strategy for disease control. The strategy will identify some localities as candidates for being isolated or for having their connections to other localities curtailed. The measure on which the identification is based is that of centrality of a node. The betweenness centrality of a node v is defined as [32]:

$$g(v) = \sum_{i \neq v \neq j} \frac{\sigma_{ij}(v)}{\sigma_{ij}}$$

where σ_{ij} is the total number of shortest paths from node i to node j passing through $\sigma_{ij}(v)$. Therefore, the more central the node is, the more its removal has an effect on the network's connectivity, since its removal would yield a network with more disconnected subgraphs. The control strategy we propose involves an iterative procedure, where at each step the centralities of the nodes are computed, the node with the resulting highest centrality is removed, and the matrix A is updated, as illustrated in Figure 12.

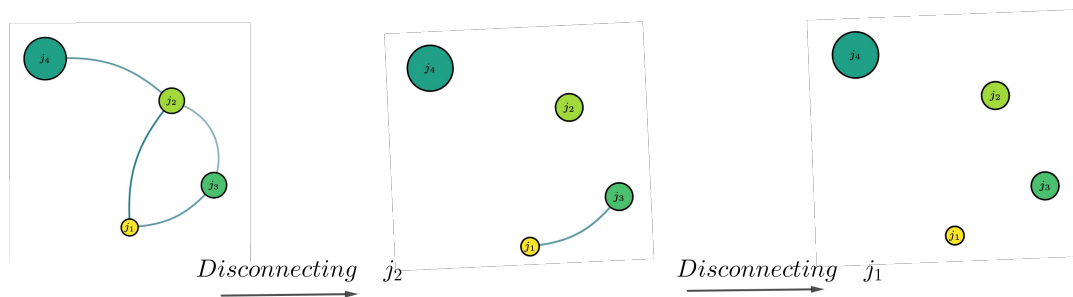


Figure 12: The figure illustrates the iterative scheme. First, the node with the highest centrality j_2 is disconnected by removing all its links, as it is the node with the highest number of shortest paths. The resulting network has j_1 and j_3 with equal centralities and either one can be disconnected. This leads to a total loss of connectivity in the network at the end of the process.

Other removal schemes of nodes in network exist, but the one we have just described has been suggested to incur the highest loss of connectivity for scale-free networks [36, 37, 38, 39, 40, 41]. In practice, candidate targets for intervention the localities corresponding to nodes with higher centralities. At the policy level this strategy was adopted. The localities we have identified through this strategy were given priority in the national vaccination campaign. On the other hand, the recommendations we put forward based on this analysis were only partially adopted in targeting the high centrality localities for lockdown and intervention measures, as the decision making process involved other ministries and stakeholders. However, we have considered the theoretical repercussions of such implementation. Clearly, the loss of connectivity will impede the evolution of the disease since the localities which are contributing the most to the infection will be isolated. For

example, removing around 20% of the most connected localities on the basis of their betweenness centrality will lead to 80% loss of connectivity as shown in Figure 13. Specifically, the localities

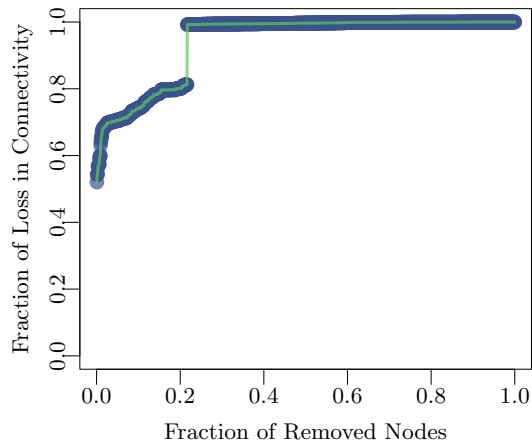


Figure 13: The loss of connectivity versus the fraction of removed nodes for the cascading and non-cascading strategies.

causing 80% loss of connectivity are shown in Figure 14, while the fitted model of the top sixteen localities is shown in Figure 15. An animated map of the control strategy is available online.

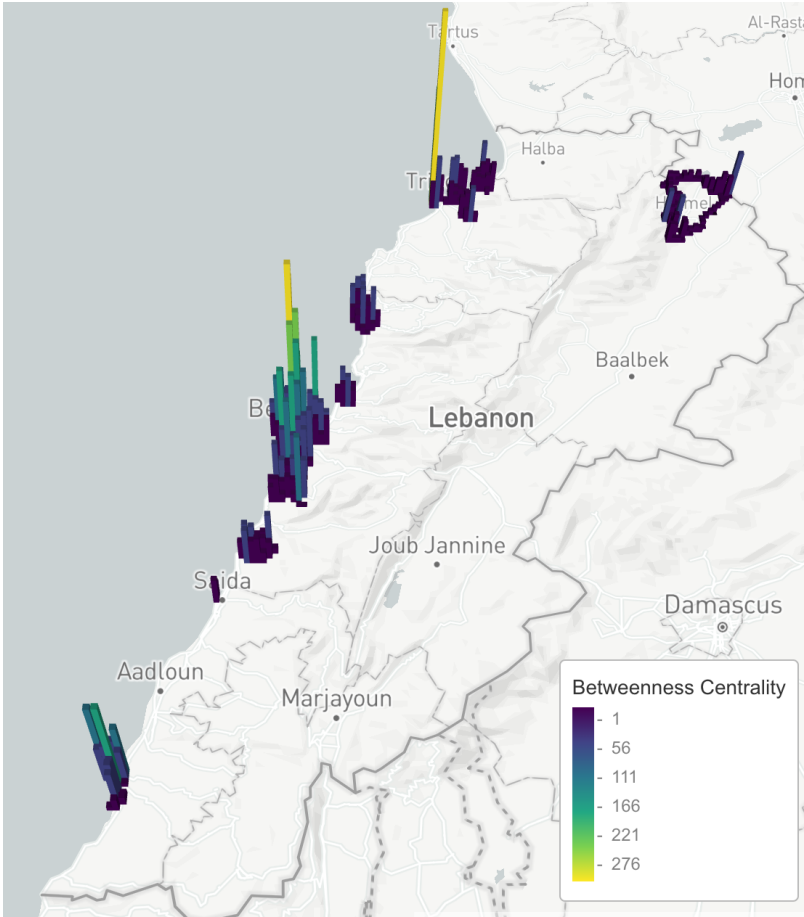


Figure 14: The map shows the localities with the highest centrality whose removals lead to 80% loss of connectivity.

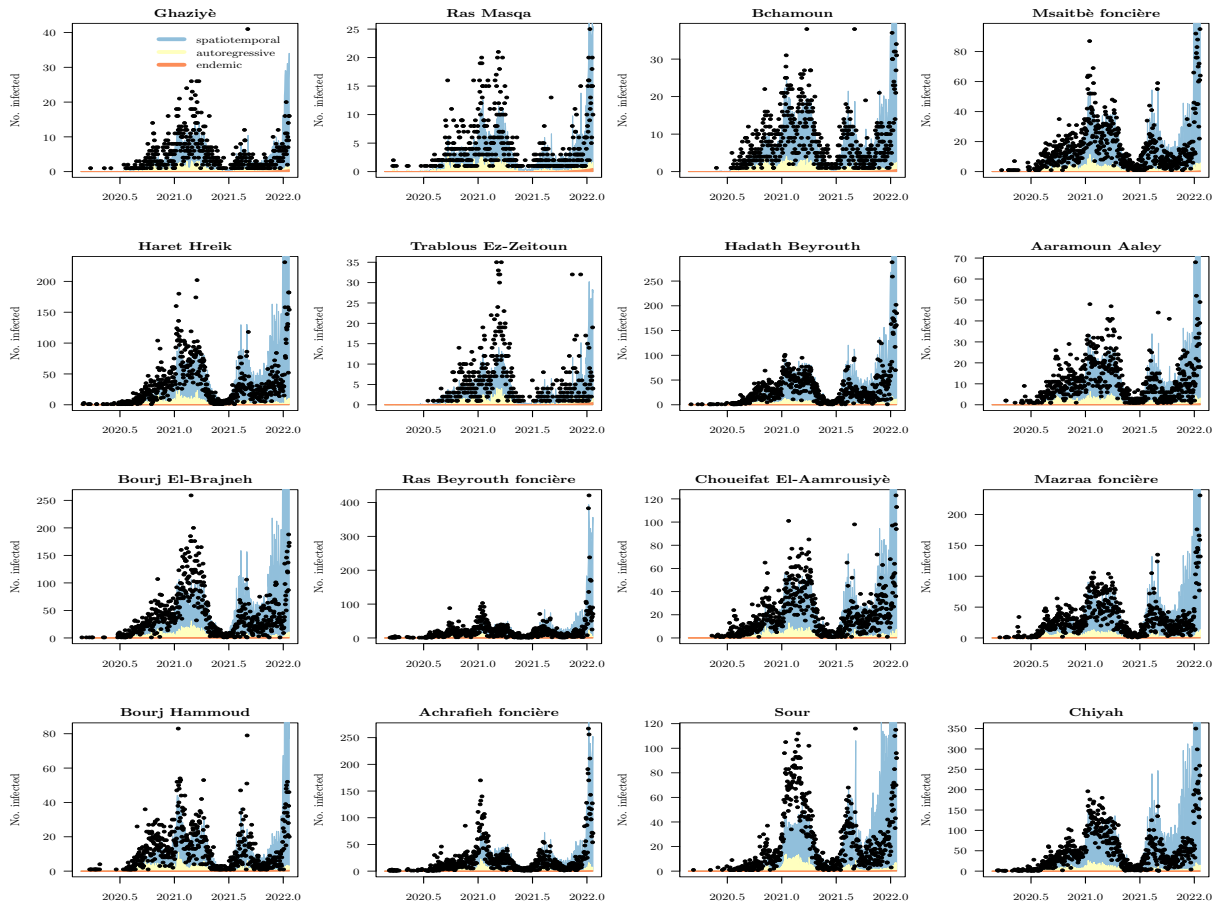


Figure 15: The figure shows the counts, along with the fitted model, for twelve localities ordered by decreasing betweenness centrality.

5 Conclusion

In this paper, we have followed the evolution of the counts of COVID-19 cases in Lebanon at the locality level at a daily resolution. The framework that we have adopted relies on an auto-regressive model fitted to contiguous 20-days intervals. We have been able to recover the underlying network over which the disease was propagating. The analysis of the topological metrics of this time-evolving network gives us a hint into a transition to a steady state structure that governs interactions between localities. After identifying this steady state network, and characterizing it as a scale-free, we have proposed control measures based on betweenness centrality of its nodes. The findings were taken into consideration in the national vaccination campaign for COVID-19, with the identified localities given priority for vaccination.

Acknowledgement

The authors acknowledge the support of Prof. Rima Habib from the AUB's Faculty of Public Health for her unfailing support and invaluable advice to physicists and mathematicians as they worked with public data as well as Dr. Chadi Abdallah for helping in the early conception of the project.

Appendix. Chronology of COVID-19 Pandemic in Lebanon

In this appendix we summarize the chronology of the COVID-19 pandemic in Lebanon from the first recorded case to February 2022. We divide this time interval into 4 periods, and highlight the main governmental interventions taken to control the spread of the disease.

Period 1 (February 2020 to June 2020). The first cases are documented. Early lockdown measures are implemented with airport closure. Testing is carried out for suspected cases, close contacts, and travelers. Cases are mainly within clusters. Aggressive contact tracing is adopted.

Period 2 (July 2020 to December 2020): The airport reopens in July 2020. The daily number of cases increases progressively and community transmission sets in. On August 4th, the Beirut blast occurs.

Period 3 (January 2021 to June 2021): The alpha variant is introduced. The case counts increase. Lockdown measures are implemented resulting in a decrease of the recorded cases. However, after lockdown release, an increase of the number of infections is observed until mid-March, with a progressive and sustained decrease up to June.

Period 4 (July 2021 to December 2021). Introduction of the delta variant, which progressively replaces the alpha variant. Two waves of delta are observed: July-September and November-December.

Period 5 (January 2022-February 2022). Introduction of the omicron variant. High transmissibility of the new variant leads to high daily case counts reaching 10,000 on 1st Feb 2022.

References

- [1] Y. Mohamadou, A. Halidou, and P. T. Kapen, "A review of mathematical modeling, artificial intelligence and datasets used in the study, prediction and management of COVID-19," Applied Intelligence, vol. 50, no. 11, pp. 3913–3925, 2020.
- [2] J. Guan, Y. Wei, Y. Zhao, and F. Chen, "Modeling the transmission dynamics of COVID-19 epidemic: a systematic review," Journal of Biomedical Research, vol. 34, no. 6, p. 422, 2020.
- [3] A. Celani and P. Giudici, "Endemic–epidemic models to understand COVID-19 spatio-temporal evolution," Spatial Statistics, p. 100528, 2021.
- [4] P. Ssentongo, C. Fronterre, A. Geronimo, S. J. Greybush, P. K. Mbabazi, J. Muvawala, S. B. Nahalamba, P. O. Omadi, B. T. Opar, S. A. Sinnar, et al., "Pan-African evolution of within- and between-country COVID-19 dynamics," Proceedings of the National Academy of Sciences, vol. 118, no. 28, 2021.

- [5] M. M. Dickson, G. Espa, D. Giuliani, F. Santi, and L. Savadori, “Assessing the effect of containment measures on the spatio-temporal dynamic of COVID-19 in Italy,” Nonlinear Dynamics, vol. 101, no. 3, pp. 1833–1846, 2020.
- [6] N. Gozzi, P. Bajardi, and N. Perra, “The importance of non-pharmaceutical interventions during the COVID-19 vaccine rollout,” medRxiv, 2021.
- [7] N. Perra, “Non-pharmaceutical interventions during the COVID-19 pandemic: A review,” Physics Reports, 2021.
- [8] D. Brockmann and D. Helbing, “The hidden geometry of complex, network-driven contagion phenomena,” science, vol. 342, no. 6164, pp. 1337–1342, 2013.
- [9] F. Schlosser and D. Brockmann, “Finding disease outbreak locations from human mobility data,” EPJ data science, vol. 10, no. 1, p. 52, 2021.
- [10] S. Zhu, A. Bukharin, L. Xie, M. Santillana, S. Yang, and Y. Xie, “High-resolution spatio-temporal model for county-level COVID-19 activity in the US,” ACM Transactions on Management Information Systems (TMIS), vol. 12, no. 4, pp. 1–20, 2021.
- [11] W.-H. Chiang, X. Liu, and G. Mohler, “Hawkes process modeling of COVID-19 with mobility leading indicators and spatial covariates,” International journal of forecasting, 2021.
- [12] P. Giudici, P. Pagnottoni, and A. Spelta, “Network self-exciting point processes to measure health impacts of COVID-19,” Available at SSRN 3892998, 2021.
- [13] L. Held, M. Höhle, and M. Hofmann, “A statistical framework for the analysis of multivariate infectious disease surveillance counts,” Statistical Modelling, vol. 5, pp. 187–199, 2005.
- [14] S. Meyer, L. Held, and M. Höhle, “Spatio-temporal analysis of epidemic phenomena using the R package surveillance,” arXiv preprint arXiv:1411.0416, 2014.
- [15] S. Meyer and L. Held, “Power-law models for infectious disease spread,” The Annals of Applied Statistics, vol. 8, no. 3, pp. 1612–1639, 2014.
- [16] M. T. Angulo, J. A. Moreno, G. Lippner, A.-L. Barabási, and Y.-Y. Liu, “Fundamental limitations of network reconstruction from temporal data,” Journal of the Royal Society Interface, vol. 14, no. 127, p. 20160966, 2017.
- [17] S. G. Shandilya and M. Timme, “Inferring network topology from complex dynamics,” New Journal of Physics, vol. 13, no. 1, p. 013004, 2011.
- [18] S. Prabakaran, J. Gunawardena, and E. Sontag, “Paradoxical results in perturbation-based signaling network reconstruction,” Biophysical journal, vol. 106, no. 12, pp. 2720–2728, 2014.
- [19] D. Yu, “Estimating the topology of complex dynamical networks by steady state control: Generality and limitation,” Automatica, vol. 46, no. 12, pp. 2035–2040, 2010.
- [20] D. Yu and U. Parlitz, “Inferring local dynamics and connectivity of spatially extended systems with long-range links based on steady-state stabilization,” Physical Review E, vol. 82, no. 2, p. 026108, 2010.

- [21] X. Wan, J. Liu, W. K. Cheung, and T. Tong, “Inferring epidemic network topology from surveillance data,” PLoS One, vol. 9, no. 6, p. e100661, 2014.
- [22] S. Pajevic and D. Plenz, “Efficient network reconstruction from dynamical cascades identifies small-world topology of neuronal avalanches,” PLoS computational biology, vol. 5, no. 1, p. e1000271, 2009.
- [23] A. Braunstein, A. Ingrosso, and A. P. Muntoni, “Network reconstruction from infection cascades,” Journal of the Royal Society Interface, vol. 16, no. 151, p. 20180844, 2019.
- [24] E. Verdeil, G. Faour, S. Velut, M. Hamzé, and F. Mermier, Atlas du LIBAN. Presses de l’Ifpo, 2007.
- [25] G. K. Zipf, “The $p \propto 1/p^2$ hypothesis: on the intercity movement of persons,” American sociological review, vol. 11, no. 6, pp. 677–686, 1946.
- [26] F. Simini, M. C. González, A. Maritan, and A.-L. Barabási, “A universal model for mobility and migration patterns,” Nature, vol. 484, no. 7392, pp. 96–100, 2012.
- [27] M. Barthélemy, “Spatial networks,” Physics Reports, vol. 499, no. 1-3, pp. 1–101, 2011.
- [28] K. Karumanagoundar, M. Raju, M. Ponnaiah, P. Kaur, P. Rubeshkumar, M. Sakthivel, P. Shanmugiah, P. Ganeshkumar, S. K. Muthusamy, M. Sendhilkumar, et al., “Secondary attack rate of COVID-19 among contacts and risk factors, tamil nadu, march–may 2020: a retrospective cohort study,” BMJ open, vol. 11, no. 11, p. e051491, 2021.
- [29] S. Fortunato, “Community detection in graphs,” Physics reports, vol. 486, no. 3-5, pp. 75–174, 2010.
- [30] P. Grindrod and D. J. Higham, “High modularity creates scaling laws,” Scientific reports, vol. 8, no. 1, pp. 1–9, 2018.
- [31] R. Albert and A.-L. Barabási, “Statistical mechanics of complex networks,” Reviews of modern physics, vol. 74, no. 1, p. 47, 2002.
- [32] M. E. Newman, “The structure and function of complex networks,” SIAM review, vol. 45, no. 2, pp. 167–256, 2003.
- [33] R. Pastor-Satorras, C. Castellano, P. Van Mieghem, and A. Vespignani, “Epidemic processes in complex networks,” Reviews of modern physics, vol. 87, no. 3, p. 925, 2015.
- [34] M. E. Newman, “Spread of epidemic disease on networks,” Physical review E, vol. 66, no. 1, p. 016128, 2002.
- [35] A. Clauset, C. R. Shalizi, and M. E. Newman, “Power-law distributions in empirical data,” SIAM review, vol. 51, no. 4, pp. 661–703, 2009.
- [36] R. Albert, H. Jeong, and A.-L. Barabási, “Error and attack tolerance of complex networks,” nature, vol. 406, no. 6794, pp. 378–382, 2000.
- [37] G. Dong, J. Gao, R. Du, L. Tian, H. E. Stanley, and S. Havlin, “Robustness of network of networks under targeted attack,” Physical Review E, vol. 87, no. 5, p. 052804, 2013.

- [38] L. D. Valdez, L. Shekhtman, C. E. La Rocca, X. Zhang, S. V. Buldyrev, P. A. Trunfio, L. A. Braunstein, and S. Havlin, “Cascading failures in complex networks,” Journal of Complex Networks, vol. 8, no. 2, p. cnaa013, 2020.
- [39] S. V. Buldyrev, R. Parshani, G. Paul, H. E. Stanley, and S. Havlin, “Catastrophic cascade of failures in interdependent networks,” Nature, vol. 464, no. 7291, pp. 1025–1028, 2010.
- [40] R. Albert, I. Albert, and G. L. Nakarado, “Structural vulnerability of the North American power grid,” Physical review E, vol. 69, no. 2, p. 025103, 2004.
- [41] P. Edsberg Møllgaard, S. Lehmann, and L. Alessandretti, “Understanding components of mobility during the COVID-19 pandemic,” Philosophical Transactions of the Royal Society A, vol. 380, no. 2214, p. 20210118, 2021.